


RESEARCH ARTICLE

[View Article Online](#)
[View Journal](#) | [View Issue](#)Cite this: *RSC Med. Chem.*, 2022, **13**, 1350Synthesis, biological evaluation and computational studies of pyrazole derivatives as *Mycobacterium tuberculosis* CYP121A1 inhibitors†Lama A. Alshabani,^a Amit Kumar,^b Sam J. Willcocks,^{cd} Gayathri Srithiran,^d Sanjib Bhakta,^d D. Fernando Estrada^b and Claire Simons^b  ^{*,a}

A series of imidazole and triazole diarylpyrazole derivatives were prepared using an efficient 5-step synthetic scheme and evaluated for binding affinity with *Mycobacterium tuberculosis* (Mtb) CYP121A1 and antimycobacterial activity against Mtb H37Rv. Antimycobacterial susceptibility was measured using the spot-culture growth inhibition assay (SPOTi): the imidazoles displayed minimum inhibitory concentration (MIC₉₀) in the range of 3.95–12.03 µg mL⁻¹ (10.07–33.19 µM) with **11f** the most active, while the triazoles displayed MIC₉₀ in the range of 4.35–25.63 µg mL⁻¹ (11.88–70.53 µM) with **12b** the most active. Assessment of binding affinity using UV-vis spectroscopy showed that for the imidazole series, the propyloxy (**11f**) and isopropoxy (**11h**) derivatives of the 4-chloroaryl pyrazoles displayed Mtb CYP121A1 type II binding affinity with K_d 11.73 and 17.72 µM respectively compared with the natural substrate cYY (K_d 12.28 µM), while in the triazole series, only the methoxy substitution with the 4-chloroaryl pyrazole (**12b**) showed good type II Mtb CYP121A1 binding affinity (K_d 5.13 µM). Protein-detected 1D ¹⁹F-NMR spectroscopy as an orthogonal strategy was used to evaluate ligand binding independent of perturbations at the haem. For imidazole and triazole compounds, perturbations were more intense than cYY indicating tighter binding and confirming that ligand coordination occurs in the substrate-binding pocket despite very modest changes in UV-vis absorbance, consistent with computational studies and the demonstrated potential anti-tuberculosis properties of these compounds.

Received 24th May 2022,
Accepted 12th August 2022

DOI: 10.1039/d2md00155a

rsc.li/medchem

Introduction

Tuberculosis (TB) was, prior to COVID-19, the leading cause of death from a single infectious agent. The impact of COVID-19 on TB has been substantial, most notably with TB resources, funding and facilities being redirected for COVID-19 and also a reduction in reporting data for newly diagnosed TB patients.¹ Reduced access to testing facilities has resulted in an increase in TB related deaths in 2020 with estimates of 1.3 million deaths in HIV-negative people and 214 000 deaths in HIV-positive people.¹ The rise in drug-resistant strains of *Mycobacterium tuberculosis* (Mtb), the main causative agent of

TB, continues to be of concern with rifampicin resistant TB (RR-TB), multidrug resistant TB (MDR-TB) which is resistant to both first line anti-TB drugs rifampicin and isoniazid, and extremely drug resistant TB (XDR-TB) which is resistant against rifampicin and any second line fluoroquinolone plus one second line injectable anti-TB drug, exacerbating the challenge of effectively treating TB.² Therefore, research looking at alternative Mtb targets, for which no resistance is already present in the population, is of interest to provide additional therapeutic drugs as part of the combinatorial drug approach used for TB treatment.

A target of interest is cytochrome P450 121A1 (CYP121A1, mycocyclusin synthase), an essential enzyme for Mtb viability,³ which catalyses the biotransformation of the tyrosine dipeptide cyclo-L-Tyr-L-Tyr (cYY) to mycocyclusin (Fig. 1).⁴ The exact role of mycocyclusin is not known, however it has been suggested that it may have an essential role in cell growth or structural stability, alternatively inhibition of CYP121A1 could result in an accumulation of cYY, which may be toxic to Mtb.^{4,5}

CYP121A1 inhibitors with a range of structural scaffolds have been described by us^{6–9} and others.^{10–12} In all cases a basic nitrogen containing group with the potential to bind to the iron of the haem group is included, although indirect water-mediated binding with the haem is occasionally

^a School of Pharmacy & Pharmaceutical Sciences, Cardiff University, King Edward VII Avenue, Cardiff, CF10 3NB UK. E-mail: simonsc@cardiff.ac.uk^b Department of Biochemistry, Jacobs School of Medicine and Biomedical Science, University at Buffalo, Buffalo, New York-14203, USA^c Department of Infection Biology, The London School of Hygiene and Tropical Medicine, London, WC1E 7HT UK^d Mycobacteria Research Laboratory, Institute of Structural and Molecular Biology, Department of Biological Sciences, Birkbeck, University of London, London WC1E 7HX, UK† Electronic supplementary information (ESI) available: Experimental methods and analytical data for compounds 7–10; NMR for compounds 11 and 12. See DOI: <https://doi.org/10.1039/d2md00155a>

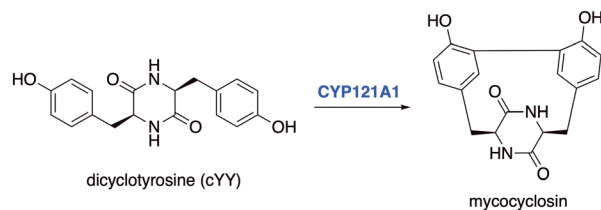


Fig. 1 Mycrocyclosin formed through a CYP121A1 mediated C–C bond formation between carbon atoms in the *ortho*-positions of two tyrosine groups in the cyclodipeptide dicyclocytosine (cYY).

observed and/or binding of the nitrogen containing group with Gln395/Arg386, which would block access of cYY to the active site.^{6–12} One of the more promising scaffolds is the diarylpyrazole series^{6,9} with optimal binding observed for imidazole as the nitrogen containing binding group and substitution of one of the aryl rings with lipophilic alkyl groups (Fig. 2).

Presented here is a further design of these lead pyrazole derivatives to consider drug likeness, incorporating *O*-alkyl substitutions in one aryl ring to improve hydrophilic properties compared with the lead compounds, and the addition of a halide (F or Cl) in the second aryl ring for metabolic stability (Fig. 2). Imidazole and 1,2,4-triazole azole moieties are included as the basic nitrogen binding groups to evaluate effect on binding affinity and antimycobacterial activity.

Results and discussion

Chemistry

The hydrazines (7) were prepared following previously described methodology^{6,9} by reaction of the 4-alkoxy-acetophenones (1–4) with either 4-fluoro or 4-chlorophenylhydrazine hydrochloride

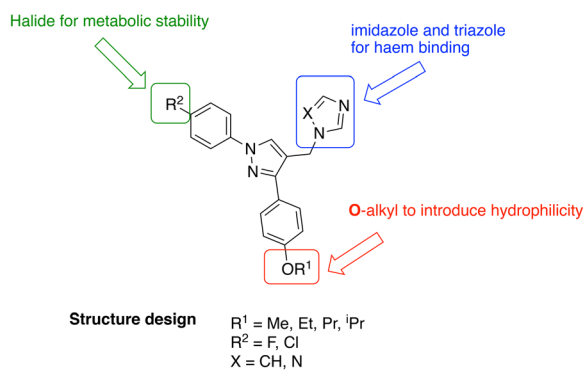
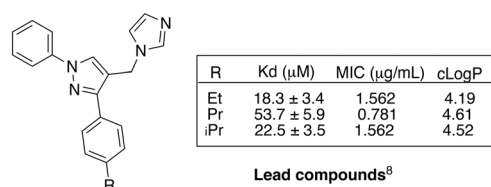
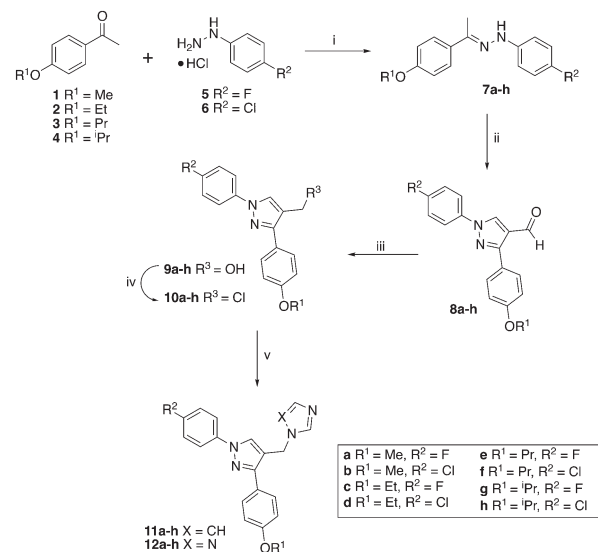


Fig. 2 Lead diarylpyrazole derivatives⁹ and structure design of new compounds to improve drug likeness.



(5 or 6) in EtOH with acetic acid as the acid catalyst (Scheme 1). The hydrazines (7) were converted to the aldehydes (8) on reaction with Vilsmeier–Haack reagent, generated *in situ* from DMF and POCl₃, and obtained as solids in good yields (65–100%).

The aldehydes (8) were reduced with NaBH₄ and the alcohols (9), obtained after extraction with EtOAc in yields of 68–98%, were converted to the chlorides (10) on treatment with SOCl₂ in CH₂Cl₂ at 40 °C for 4 h. The crude chlorides (10) were obtained in very high yields (93–100%) except for the isopropyl/fluoride derivative (48%), and were used immediately in the next reaction, which involved the generation of the imidazole or triazole anion by reaction of imidazole or triazole with K₂CO₃ in CH₃CN at 45 °C for 1 h, followed by the addition of the chlorides and heating at 70 °C overnight (Scheme 1). The final

Table 1 Yields and mp data for imidazoles (11) and triazoles (12)

Compd	R ¹	R ²	X	Yield (%)	m.p. (°C)
11a	Me	F	CH	70	150–152
11b	Me	Cl	CH	61	136–138
11c	Et	F	CH	45	118–120
11d	Et	Cl	CH	22	124–126
11e	Pr	F	CH	66	120–122
11f	Pr	Cl	CH	63	90–92
11g	iPr	F	CH	58	96–98
11h	iPr	Cl	CH	94	98–100
12a	Me	F	N	58	150–152
12b	Me	Cl	N	60	124–126
12c	Et	F	N	52	140–142
12d	Et	Cl	N	60	122–124
12e	Pr	F	N	58	120–122
12f	Pr	Cl	N	72	114–116
12g	iPr	F	N	53	118–120
12h	iPr	Cl	N	81	98–100

imidazole (**11**) and triazole (**12**) products were obtained after purification by gradient column chromatography with generally good yields (Table 1).

Antimycobacterial activity (MIC₉₀)

All compounds were evaluated for MIC₉₀ against Mtb H37Rv using the SPOTi assay as previously described.¹³ The imidazoles all showed good antimycobacterial activity (Table 2) with optimal activity observed for the propyloxy/Cl (**11f**, MIC₉₀ 4.0 µg mL⁻¹, 10.1 µM) and isopropyloxy/F (**11h**, MIC₉₀ 4.4 µg mL⁻¹, 11.9 µM) derivatives. The activity observed for all the imidazole derivatives (except **11c**) and the triazoles **12b**, **12d** and **12f** was comparable with the standard kanamycin (MIC₉₀ 7.8 µg mL⁻¹, 16.1 µM), which is an important second line drug for the treatment of MDR-TB.¹⁴

Mtb CYP121A1 binding affinity

All sixteen final compounds (**11a–h** and **12a–h**) were subject to a preliminary binding affinity screen, which identified seven imidazole (**11a**, **11c–h**) and one triazole derivatives (**12b**) for further evaluation. Evaluation of inhibitor affinity was carried out in a 96-well plate format. The K_d of cYY in this assay (12 µM) was consistent with its previously reported value.^{4,16} As a comparison, all inhibitors were titrated manually in a 1 cm quartz cuvette for a single trial. The calculated K_d values closely matched the results from the plate-reader assay.

The methoxy triazole derivative with a chloroaryl group (**12b**) displayed the tightest binding affinity with K_d 5.1 ± 1.5 µM, and in the imidazole series the derivatives with a chloroaryl group were generally more effective in binding to Mtb CYP121A1 compared with the compounds with a fluoroaryl group. The propyloxy derivative (**11f**, K_d 11.7 ± 5.4

Table 3 Mtb CYP121A1 binding affinity and Soret band shift

Compd	CYP121A1 K _d (µM)	Soret shift (nm)
11a	65.0 ± 16.6	417 to 421
11c	54.0 ± 5.2	417 to 422
11d	18.8 ± 10.2	417 to 420
11e	22.3 ± 4.2	417 to 420
11f	11.7 ± 5.4	417 to 419
11g	38.5 ± 8.7	417 to 419
11h	17.7 ± 6.9	417 to 419
12b	5.1 ± 1.5	417 to 417
cYY	12.3 ± 1.1	417 to 395

µM) displayed binding affinity comparable with cYY (K_d 12.3 ± 1.1 µM) (Table 3).

As previously stated cYY in the co-crystal structure displays indirect binding with the haem *via* interstitial water molecules.^{4,16}

However, absorbance changes from cYY titration in solution produce a typical type-I spectral response, indicating displacement of the haem water molecule(s) and induction of a high-spin form of the iron. The pyrazoles described here displayed a type II binding profile suggesting direct binding with the haem (Fig. 3 and S1 and S2†).

In the co-crystal structure with cYY, CYP121A1 coordinates the substrate within the active site while also preserving the space and hydrogen-bonding necessary to maintain a two-molecule water bridge to the haem.⁴ CYP121A1 is also known to coordinate the inhibitor fluconazole concomitantly with the haem water ligand.¹⁷ In practice, such coordination is difficult to detect by absorbance difference spectra alone, which rely on ligand-induced displacement of the water molecule followed by direct azole ligation to the haem. In light of this possibility, protein-detected 1D ¹⁹F-NMR spectroscopy was utilised as an orthogonal strategy to evaluate ligand binding independent of perturbations at the haem. As described recently,¹⁸ BTFA labelling of an S171C mutation located within the CYP121A1 FG-loop serves as a direct reporter of protein–ligand interactions. The FG-loop in CYPs is known to undergo extensive structural remodelling in response to ligand binding.^{19–21} In ligand-free CYP121A1, the conformational heterogeneity of the loop is indicated by at least three separate resonances (Fig. 4). As reported previously,¹⁸ a 3-fold addition of

Table 2 MIC₉₀ of compounds against Mtb H37Rv

Compd	MIC ₉₀ ^a (µg mL ⁻¹)	MIC ₉₀ ^a (µM)	cLog P ^b
11a	4.3	12.3	3.32
11b	6.0	16.5	3.72
11c	12.0	33.2	3.66
11d	5.0	13.3	4.06
11e	6.0	15.9	4.15
11f	4.0	10.1	4.55
11g	4.3	11.4	3.98
11h	6.0	15.3	4.38
12a	12.8	36.7	2.83
12b	4.4	11.9	3.23
12c	25.6	70.5	3.17
12d	6.4	16.8	3.57
12e	20.9	55.5	3.65
12f	6.4	16.2	4.05
12g	20.9	55.5	3.49
12h	25.6	65.1	3.89
Isoniazid	0.2	1.8	-0.64
Kanamycin	7.8	16.1	-7.58
Rifampicin	0.2	0.3	—

^a Results are the average of two independent experiments.

^b Crippen's fragmentation.¹⁵

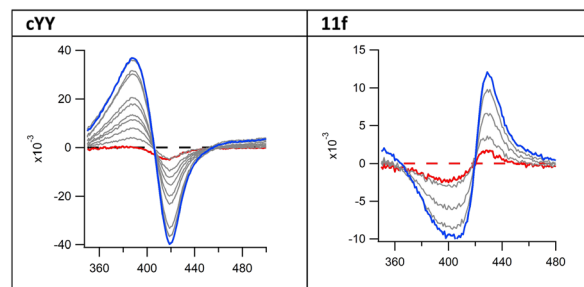


Fig. 3 Binding difference spectra of cYY (type I) and pyrazole exemplar **11f** (type II).



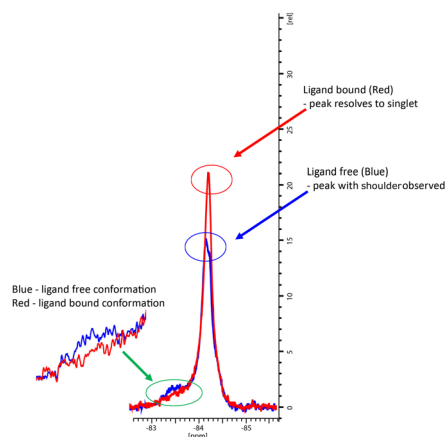


Fig. 4 ^{19}F NMR spectra of BTFA-labelled CYP121_S171C (blue) alone and with cYY bound (red).

cYY reduces the intensity of the broad down-field resonance at -83.5 ppm while increasing the intensity of the major upfield resonance near -84.5 ppm, thus indicating reduced heterogeneity of the FG-loop conformation and an increase in the ligand-bound state (Fig. 4).

To evaluate the interaction with the compounds, ^{19}F -NMR spectra were acquired for BTFA-labelled CYP121_S171C in the presence of 3-fold excess concentrations of representative imidazole and triazole derivatives. For comparison, spectra were overlayed with ligand-free and cYY-bound spectra recorded from samples from the same batch of labelled protein and at matching protein concentrations.

As expected, the perturbations induced by the imidazole derivatives **11a** and **11g** are consistent with an interaction that occurs within the CYP121 active site, since both compounds elicit similar changes in the NMR spectrum of the FG-loop when compared to cYY (Fig. 5A and B). Moreover, the relative extent of these perturbations aligns with the change in the Soret peak of absorbance assays (Table 3). Interestingly, NMR spectra recorded in the presence of the triazole derivatives **12b** and **12d**

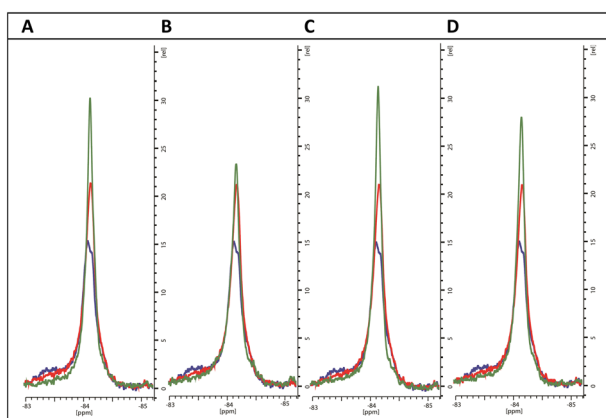


Fig. 5 ^{19}F NMR spectra of BTFA-labelled CYP121_S171C (blue) alone, with cYY bound (red) and with exemplar pyrazole ligands (green) (A) **11a**, (B) **11g**, (C) **12b** and (D) **12d**.

were generally not in agreement with the absorbance data. These compounds elicited a weak spectral response in the UV-vis assay when compared with the imidazole derivatives. However, their presence induced all the characteristic changes of ligand-binding in ^{19}F -NMR spectra. For both compounds, perturbations were more intense than that of cYY (Fig. 5C and D). Our interpretation of this apparent disagreement in binding behaviour is that weaker triazole-coordination of the haem may also allow for preservation of the haem-coordinated water ligand, as indicated by weaker absorbance data overall, and similar to the non-haem binding mode observed with fluconazole. Hence, the detection of ligand-binding by ^{19}F -NMR, and thus confirmation that ligand coordination occurs in the substrate-binding pocket despite very modest changes in absorbance, is consistent with the demonstrated growth inhibition potential of these compounds.

Computational studies

Mtb CYP121A1 protein-ligand complexes were generated through docking of compounds **11** and **12** with the crystal structure of Mtb CYP121A1 co-crystallised with cYY (pdb 3G5H⁴) using Molecular Operating Environment (MOE) software.²² The protein-ligand complexes were then subject to 150 ns molecular dynamics (MD) simulations using the Desmond programme of Schrödinger software.²³

cYY sits to one side of the haem and is tethered through a H-bonding interaction between one phenolic OH and Arg386 on one side of the active site and through H-bonding interactions between the diketopiperazine ring C=O and NH groups with Val83 and Asn85 on the opposite side of the active site (Fig. 6).

All the pyrazole derivatives were positioned in a comparable position occupied by cYY, to the side of the haem group (Fig. 7). Water-mediated binding interactions were observed with either the imidazole, triazole or pyrazole ring with Gln385/Arg386 and additional hydrophobic/ π - π stacking between one of the benzene rings of the pyrazole and Phe168 (e.g. **11b**, **12b** and **12d**) (Fig. 8). A halide interaction was observed for some of the pyrazole derivatives with Leu73 (e.g.

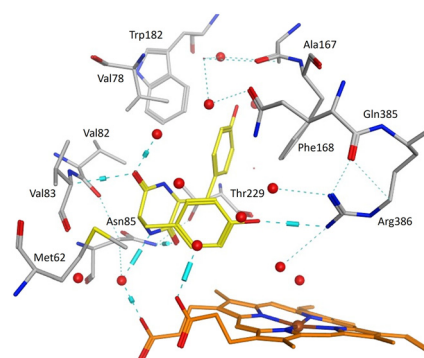


Fig. 6 cYY (yellow) binding in Mtb CYP121A1 active site (pdb 3G5H). Haem shown in orange, water molecules as red spheres, H-bonding as blue lines/cylinders.



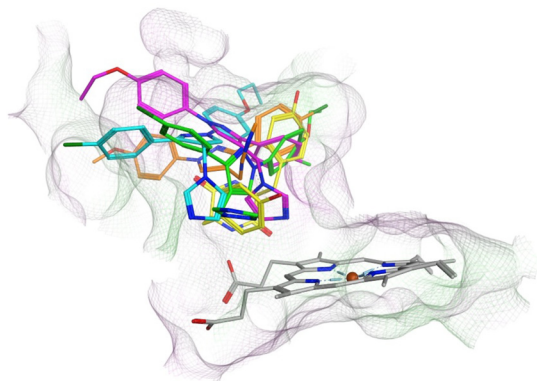


Fig. 7 Comparison of binding position of pyrazoles **11c** (magenta), **11f** (cyan), **12b** (orange) and **12d** (green) with cYY (yellow).

11b and **12d**) and additional water mediated and multiple hydrophobic interactions (Fig. 8).

Conclusions

In this pyrazole series, the imidazole derivatives were generally more active against Mtb with optimal activity observed for the longer/branched chain alkoxy substitutions

(*e.g.* **11f** and **11g**). For the triazole derivatives, the compounds with a chlorobenzene ring were more active against Mtb compared with triazole derivatives containing a fluorobenzene ring. Generally, UV-vis spectral binding assay, which measures binding to the haem, either direct (type II) or indirect (type I through displacement of the 6th axial water ligand of the haem, confirmed type II binding for the imidazole derivatives and reflected Mtb inhibitory (MIC) activity. Compared with lead imidazole compounds (Fig. 2), binding affinity was either comparable or improved but the Mtb inhibitory activity was reduced (*e.g.* Fig. 2, lead compound R = Pr MIC $0.78 \mu\text{g mL}^{-1}$ compared with propyloxy derivative **11f** MIC $4.0 \mu\text{g mL}^{-1}$). Possibly the reduction in lipophilicity compared with the lead compounds, owing to addition of the oxygen from the alkoxy substitution may be sufficient to reduce uptake across the Mtb cell membrane.

Previously we prepared methoxy derivatives with both imidazole and triazole haem binding groups (P1 and P2, Table 4), both of which had $\text{MIC}_{90} = 25 \mu\text{g mL}^{-1}$.⁶ Comparison with the methoxy derivatives (**11a–b**, **12a–b**) with the halide substitutions in the second aryl ring showed improved antimycobacterial activity, which may also be related to the increase in lipophilicity and would be consistent with our previous studies.^{6–9}

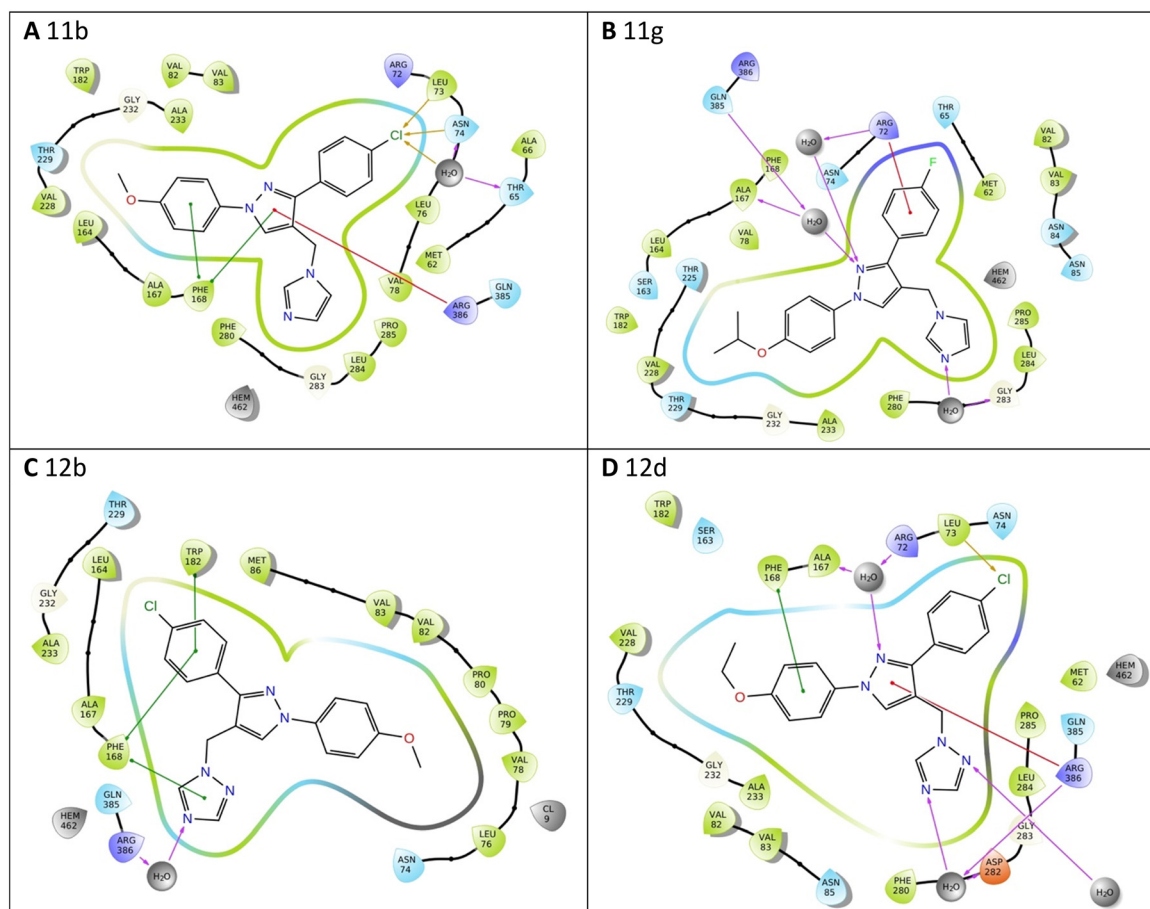
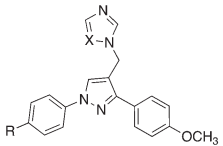


Fig. 8 Exemplar 2D ligand interactions with Mtb CYP121A1. (A) **11b**, (B) **11g**, (C) **12b** and (D) **12d**.



Table 4 MIC₉₀ of methoxy compounds against Mtb H37Rv


Compd	R	X	MIC ₉₀ ^a (μg mL ⁻¹)	cLog P ^b
P1	H	CH	25	3.16
11a	F	CH	4.3	3.32
11b	Cl	CH	6.0	3.72
P2	H	N	25	2.67
12a	F	N	12.8	2.83
12b	Cl	N	4.4	3.23

^a Results are the average of two independent experiments. ^b Crippen's fragmentation.¹⁵

Only one triazole (**12b**) had a measurable binding affinity using the UV-vis spectral assay, which did not correlate with the Mtb inhibitory activity observed (MIC). The use of the ¹⁹F NMR assay to measure changes observed in the FG loop upon binding of ligands using BTFA ¹⁹F labelled CYP121_S171C, provided support that for the triazole derivatives (and imidazole derivatives) ligand coordination occurs in the substrate-binding pocket and in all cases with tighter binding than cYY (Fig. 5). Computational studies also support the pyrazole compounds binding in the substrate (cYY) binding pocket (Fig. 7) at the side of the haem rather than perpendicular, which may for some derivatives mean that binding or displacement of the haem water ligand may not occur even though binding in the substrate and access channel is efficient. If no perturbation of the haem/water ligand occurs this reduces the suitability of the UV-vis absorption method and highlights the importance of the results of the ¹⁹F NMR assay, which support the use of this method as an additional qualitative assay to determine ligand-CYP121A1 binding. This manuscript describes active triazole derivatives with good MIC values (some comparable with or better than the equivalent imidazole), which was not previously observed^{6–9} and, having established 1D ¹⁹F-NMR spectroscopy as an orthogonal strategy to evaluate ligand binding independent of perturbations at the haem, binding can now be confirmed. Further studies will focus on pyrazole derivative containing a triazole or alternative N-containing heterocycles (e.g. pyridines) as the haem binding moiety, as well as selectivity (human CYP panel) and toxicity assays.

Experimental

General

All chemicals, reagents and solvents were purchased from Sigma-Aldrich, Alfa Aesar, VWR, Acros and Fluka. Solvents were dried prior to use over molecular sieves (4 Å). For column chromatography, a glass column was slurry packed in the appropriate eluent with silica gel (Fluka Kieselgel 60). TLC was performed on pre-coated silica plates (dimension 20 × 20 cm) (ALUGRAM® SIL G/UV₂₅₄) with visualisation *via* UV

light (254 nm). Melting points were determined on an electrothermal instrument (Gallenkamp) and were uncorrected. ¹H, ¹³C, and ¹⁹F NMR spectra were recorded on a Bruker Advance DP500 spectrometer operating at 500, 125 and 470 MHz, respectively. Chemical shifts are given in parts per million (ppm) relative to the internal standard tetramethylsilane (Me₄Si). Elemental analysis was performed by MEDAC Ltd (Chobham, Surrey, UK) and HPLC-HRMS was performed at the Department of Pharmacy & Pharmacology, University of Bath, Bath, UK. on a Zorbax Eclipse Plus C18 Rapid Resolution 2.1 × 50 mm, 1.8 μm particle size using a 7.5 minutes gradient method 5:95 v/v water:methanol with 0.1% formic acid as additive. Experimental data for compounds **7**, **8**, **9** and **10** are provided in ESI.†

Chemistry

General procedure for the preparation of imidazole and triazole derivatives (11 and 12) from the chloride derivatives (10). To a stirred suspension of K₂CO₃ (4 equiv.) in dry CH₃CN (2.5 mL mmol⁻¹) was added imidazole or triazole (4 equiv.). The reaction mixture was heated at 45 °C for 1 h. After cooling to room temperature, the chloro derivative (**10**) (1 equiv.) was added and the reaction mixture heated at 70 °C overnight. The solvent was evaporated under reduced pressure and the resulting mixture was diluted with EtOAc (50 mL) and washed with brine (3 × 20 mL) and H₂O (3 × 20 mL). The organic layer was dried (MgSO₄) and evaporated under reduced pressure to give the crude product, which was purified by gradient column chromatography (CH₂Cl₂–MeOH).

4-((1H-Imidazol-1-yl)methyl)-1-(4-fluorophenyl)-3-(4-methoxyphenyl)-1H-pyrazole (11a). Prepared from 4-(chloromethyl)-1-(4-fluorophenyl)-3-(4-methoxyphenyl)-1H-pyrazole (**10a**) (0.5 g, 1.6 mmol). The pure compound was eluted with CH₂Cl₂–MeOH 97:3 v/v and obtained as a light brown solid. Yield 0.39 g (70%), m.p. 150–152 °C, TLC (CH₂Cl₂–MeOH 95:5 v/v) R_f 0.50. ¹H NMR (DMSO-d₆): δ 8.49 (s, 1H, pyrazole), 7.90 (m, 2H, Ar), 7.65 (s, 1H, imidazole), 7.56 (d, J = 8.5 Hz, 2H, Ar), 7.37 (m, 2H, Ar), 7.12 (s, 1H,



imidazole), 7.02 (d, $J = 9.0$ Hz, 2H, Ar), 6.89 (s, 1H, imidazole), 5.27 (s, 2H, CH₂-imidazole), 3.81 (s, 3H, OCH₃). ¹⁹F NMR (DMSO-d₆): -116.49 (F-Ar). ¹³C NMR (DMSO-d₆): δ 159.81 and 161.74 (d, $^1J_{CF} = 242.7$ Hz, C-F, Ar), 159.76 (C, Ar), 150.69 (C, pyrazole), 137.45 (CH, imidazole), 136.41 (d, $^4J_{CF} = 2.5$ Hz, C, Ar), 130.14 (CH, pyrazole), 129.22 (2 \times CH, Ar), 129.08 (CH, imidazole), 125.20 (C, Ar), 120.76 and 120.82 (d, $^3J_{CF} = 7.5$ Hz, 2 \times CH, Ar), 119.61 (CH, imidazole), 116.95 (C, pyrazole), 116.67 and 116.85 (d, $^2J_{CF} = 22.6$ Hz, 2 \times CH, Ar), 114.61 (2 \times CH, Ar), 55.64 (OCH₃), 40.95 (CH₂). Anal. calcd. for C₂₀H₁₇FN₄O (348.3814): C 68.59%, H 4.89%, N 15.99%. Found: C 68.54%, H 4.73%, N 16.07%.

4-((1*H*-Imidazol-1-yl)methyl)-1-(4-chlorophenyl)-3-(4-methoxyphenyl)-1*H*-pyrazole (11b). Prepared from 4-(chloromethyl)-1-(4-chlorophenyl)-3-(4-methoxyphenyl)-1*H*-pyrazole (**10b**) (0.35 g, 1.05 mmol). The pure compound was eluted with CH₂Cl₂-MeOH 97:3 v/v and obtained as a light orange solid. Yield 0.23 g (61%), m.p. 136–138 °C, TLC (CH₂-Cl₂-MeOH 95:5 v/v) R_f 0.44. ¹H NMR (DMSO-d₆): δ 8.53 (s, 1H, pyrazole), 7.90 (d, $J = 9.0$ Hz, 2H, Ar), 7.65 (s, 1H, imidazole), 7.58 (d, $J = 9.0$ Hz, 2H, Ar), 7.56 (d, $J = 9.0$ Hz, 2H, Ar), 7.12 (s, 1H, imidazole), 7.02 (d, $J = 9.0$ Hz, 2H, Ar), 6.88 (s, 1H, imidazole), 5.28 (s, 2H, CH₂-imidazole), 3.81 (s, 3H, CH₂CH₃). ¹³C NMR (DMSO-d₆): δ 159.83 (C, Ar), 150.94 (C, pyrazole), 138.60 (C, Ar), 137.47 (CH, imidazole), 130.86 (C, Ar), 130.10 (CH, imidazole), 129.96 (2 \times CH, Ar), 129.25 (2 \times CH, Ar), 129.08 (CH, pyrazole), 125.06 (C, pyrazole), 120.33 (2 \times CH, Ar), 119.63 (CH, imidazole), 117.32 (C, Ar), 114.63 (2 \times CH, Ar), 55.65 (CH₃), 40.94 (CH₂). Anal. calcd. for C₂₀H₁₇ClN₄O (364.8330): C 65.84%, H 4.70%, N 15.35%. Found: C 65.97%, H 4.59%, N 15.38%.

4-((1*H*-Imidazol-1-yl)methyl)-3-(4-ethoxyphenyl)-1-(4-fluorophenyl)-1*H*-pyrazole (11c). Prepared from 4-(chloromethyl)-3-(4-ethoxyphenyl)-1-(4-fluorophenyl)-1*H*-pyrazole (**10c**) (0.295 g, 0.89 mmol). The pure compound was eluted with CH₂Cl₂-MeOH 98:2 v/v and obtained as a light brown solid. Yield 0.146 g (45%), m.p. 118–120 °C, TLC (CH₂-Cl₂-MeOH 95:5 v/v) R_f 0.47. ¹H NMR (DMSO-d₆): δ 8.48 (s, 1H, pyrazole), 7.90 (dd, $J = 4.5, 9.0$ Hz, 2H, Ar), 7.64 (s, 1H, imidazole), 7.55 (d, $J = 9.0$ Hz, 2H, Ar), 7.37 (t, $J = 8.5$ Hz, 2H, Ar), 7.12 (s, 1H, imidazole), 7.0 (d, $J = 8.5$ Hz, 2H, Ar), 6.88 (s, 1H, imidazole), 5.27 (s, 2H, CH₂-imidazole), 4.07 (q, $J = 7.0$ Hz, 2H, CH₂CH₃), 1.35 (t, $J = 7.0$ Hz, 3H, CH₂CH₃). ¹⁹F NMR (DMSO-d₆): -116.52 (F-Ar). ¹³C NMR (DMSO-d₆): δ 159.80 and 161.73 (d, $^1J_{CF} = 242.7$ Hz, C-F, Ar), 159.04 (C, Ar), 150.71 (C, pyrazole), 136.42 (d, $^4J_{CF} = 2.5$ Hz, C, Ar), 130.10 (CH, pyrazole), 129.22 (2 \times CH, Ar), 129.08 (CH, imidazole), 125.06 (C, Ar), 120.74 and 120.81 (d, $^3J_{CF} = 8.8$ Hz, 2 \times CH, Ar), 119.61 (CH, imidazole), 116.96 (C, pyrazole), 116.67 and 116.85 (d, $^2J_{CF} = 22.6$ Hz, 2 \times CH, Ar), 115.04 (2 \times CH, Ar), 63.57 (CH₂CH₃), 40.96 (CH₂), 15.12 (CH₂CH₃). Anal. calcd. for C₂₁H₁₉FN₄O (362.4084): C 69.25%, H 5.26%, N 15.38%. Found: C 68.86%, H 5.06%, N 15.16%.

4-((1*H*-Imidazol-1-yl)methyl)-1-(4-chlorophenyl)-3-(4-ethoxyphenyl)-1*H*-pyrazole (11d). Prepared from 4-(chloromethyl)-1-(4-chlorophenyl)-3-(4-ethoxyphenyl)-1*H*-

pyrazole (**10d**) (0.17 g, 0.49 mmol). The pure compound was eluted with CH₂Cl₂-MeOH 97.5:2.5 v/v and obtained as a white solid. Yield 0.04 g (22%), m.p. 124–126 °C, TLC (CH₂-Cl₂-MeOH 95:5 v/v) R_f 0.55. ¹H NMR (DMSO-d₆): δ 8.53 (s, 1H, pyrazole), 7.90 (d, $J = 9.0$ Hz, 2H, Ar), 7.64 (s, 1H, imidazole), 7.58 (d, $J = 9.0$ Hz, 2H, Ar), 7.56 (d, $J = 8.8$ Hz, 2H, Ar), 7.12 (s, 1H, imidazole), 7.01 (d, $J = 8.8$ Hz, 2H, Ar), 6.88 (s, 1H, imidazole), 5.28 (s, 2H, CH₂-imidazole), 4.08 (q, $J = 7.0$ Hz, 2H, CH₂CH₃), 1.35 (t, $J = 7.0$ Hz, 3H, CH₂CH₃). ¹³C NMR (DMSO-d₆): δ 159.11 (C, Ar), 150.95 (C, pyrazole), 138.61 (C, Ar), 137.47 (CH, imidazole), 130.83 (C, Ar), 130.06 (CH, imidazole), 129.96 (2 \times CH, Ar), 129.24 (2 \times CH, Ar), 129.09 (CH, pyrazole), 124.93 (C, pyrazole), 120.31 (2 \times CH, Ar), 119.63 (CH, imidazole), 117.34 (C, Ar), 115.06 (2 \times CH, Ar), 63.58 (CH₂CH₃), 40.96 (CH₂), 15.11 (CH₂CH₃). HPLC: 97.8%, RT = 4.48 min. HRMS (ESI) m/z : calculated, 401.1145 [M + Na]⁺, Found, 401.1147 [M + Na]⁺.

4-((1*H*-Imidazol-1-yl)methyl)-1-(4-fluorophenyl)-3-(4-propoxyphenyl)-1*H*-pyrazole (11e). Prepared from 4-(chloromethyl)-1-(4-fluorophenyl)-3-(4-propoxyphenyl)-1*H*-pyrazole (**10e**) (0.30 g, 0.87 mmol). The pure compound was eluted with CH₂Cl₂-MeOH 98:2 v/v and obtained as a light orange solid. Yield 0.20 g (66%), m.p. 120–122 °C, TLC (CH₂-Cl₂-MeOH 95:5 v/v) R_f 0.51. ¹H NMR (DMSO-d₆): δ 8.48 (s, 1H, pyrazole), 7.90 (m, 2H, Ar), 7.64 (s, 1H, imidazole), 7.56 (d, $J = 9.0$ Hz, 2H, Ar), 7.36 (t, $J = 9.0$ Hz, 2H, Ar), 7.12 (s, 1H, imidazole), 7.02 (d, $J = 8.50$ Hz, 2H, Ar), 6.88 (s, 1H, imidazole), 5.27 (s, 2H, CH₂-imidazole), 3.97 (t, $J = 6.5$ Hz, 2H, OCH₂), 1.76 (m, 2H, CH₂), 1.0 (t, $J = 7.0$ Hz, 3H, CH₃). ¹⁹F NMR (DMSO-d₆): -116.51 (F-Ar). ¹³C NMR (DMSO-d₆): δ 159.80 and 161.73 (d, $^1J_{CF} = 242.7$ Hz, C-F, Ar), 159.20 (C, Ar), 150.71 (C, pyrazole), 137.45 (CH, imidazole), 136.42 (d, $^4J_{CF} = 2.5$ Hz, C, Ar), 130.10 (CH, pyrazole), 129.21 (2 \times CH, Ar), 129.08 (CH, imidazole), 125.05 (C, Ar), 120.81 and 120.74 (d, $^3J_{CF} = 8.8$ Hz, 2 \times CH, Ar), 119.62 (CH, imidazole), 116.96 (C, pyrazole), 116.67 and 116.85 (d, $^2J_{CF} = 22.6$ Hz, 2 \times CH, Ar), 115.08 (2 \times CH, Ar), 69.46 (OCH₂), 40.96 (imidazole-CH₂), 22.50 (CH₂), 10.87 (CH₃). Anal. calcd. for C₂₂H₂₁FN₄O (376.4354): C 70.20%, H 5.62%, N 14.88%. Found: C 70.00%, H 5.54%, N 14.97%.

4-((1*H*-Imidazol-1-yl)methyl)-1-(4-chlorophenyl)-3-(4-propoxyphenyl)-1*H*-pyrazole (11f). Prepared from 4-(chloromethyl)-1-(4-chlorophenyl)-3-(4-propoxyphenyl)-1*H*-pyrazole (**10f**) (0.30 g, 0.83 mmol). The pure compound was eluted with CH₂Cl₂-MeOH 98:2 v/v and obtained as a light brown solid. Yield 0.20 g (63%), m.p. 90–92 °C, TLC (CH₂Cl₂-MeOH 95:5 v/v) R_f 0.60. ¹H NMR (DMSO-d₆): δ 8.53 (s, 1H, pyrazole), 7.91 (d, $J = 9.0$ Hz, 2H, Ar), 7.65 (s, 1H, imidazole), 7.58 (d, $J = 9.0$ Hz, 2H, Ar), 7.56 (d, $J = 8.50$ Hz, 2H, Ar), 7.12 (s, 1H, imidazole), 7.02 (d, $J = 9.0$ Hz, 2H, Ar), 6.89 (s, 1H, imidazole), 5.28 (s, 2H, CH₂-imidazole), 3.98 (t, $J = 6.5$ Hz, 2H, OCH₂), 1.76 (m, 2H, CH₂), 1.0 (t, $J = 7.0$ Hz, 3H, CH₃). ¹³C NMR (DMSO-d₆): δ 159.27 (C, Ar), 150.95 (C, pyrazole), 138.61 (C, Ar), 137.48 (CH, imidazole), 130.83 (C, Ar), 130.05 (CH, imidazole), 129.95 (2 \times CH, Ar), 129.24 (2 \times CH, Ar), 129.10 (CH, pyrazole), 124.93 (C, pyrazole), 120.30 (2 \times CH,



Ar) 119.63 (CH, imidazole), 117.34 (C, Ar), 115.09 (2 × CH, Ar), 69.46 (OCH₂), 40.97 (imidazole-CH₂), 22.50 (CH₂), 10.87 (2 × CH₃). Anal. calcd. for C₂₂H₂₁ClN₄O (392.1404): C 67.26%, H 5.39%, N 14.25%. Found: C 67.25%, H 5.19%, N 14.27%.

4-((1*H*-Imidazol-1-yl)methyl)-1-(4-fluorophenyl)-3-(4-isopropoxyphenyl)-1*H*-pyrazole (11g). Prepared from 4-(chloromethyl)-1-(4-fluorophenyl)-3-(4-isopropoxyphenyl)-1*H*-pyrazole (**10g**) (0.15 g, 0.44 mmol). The pure compound was eluted with CH₂Cl₂-MeOH 98.5:1.5 v/v and obtained as a light brown solid. Yield 0.096 g (58%), m.p. 96–98 °C, TLC (CH₂Cl₂-MeOH 95:5 v/v) R_f 0.44. ¹H NMR (DMSO-*d*₆): δ 8.48 (s, 1H, pyrazole), 7.90 (m, 2H, Ar), 7.65 (s, 1H, imidazole), 7.54 (d, *J* = 9.0 Hz, 2H, Ar), 7.36 (t, *J* = 9.0 Hz, 2H, Ar), 7.13 (s, 1H, imidazole), 7.0 (d, *J* = 9.0 Hz, 2H, Ar), 6.89 (s, 1H, imidazole), 5.27 (s, 2H, CH₂-imidazole), 4.67 (m, 1H, CH), 1.30 (d, *J* = 6.0 Hz, 6H, 2CH₃). ¹⁹F NMR: (DMSO-*d*₆): -116.52 (F-Ar). ¹³C NMR (DMSO-*d*₆): δ 159.80 and 161.73 (d, ¹*J*_{CF} = 242.7 Hz, C-F, Ar), 157.99 (C, Ar), 150.72 (C, pyrazole), 137.46 (CH, imidazole), 136.43 (d, ⁴*J*_{CF} = 2.5 Hz, C, Ar), 130.06 (CH, pyrazole), 129.26 (2 × CH, Ar), 129.08 (CH, imidazole), 124.89 (C, Ar), 120.79 and 120.72 (d, ³*J*_{CF} = 8.8 Hz, 2 × CH, Ar), 119.63 (CH, imidazole), 116.96 (C, pyrazole), 116.85 and 116.67 (d, ²*J*_{CF} = 22.6 Hz, 2 × CH, Ar), 116.12 (2 × CH, Ar), 69.67 (CH), 40.97 (CH₂), 22.29 (2 × CH₃). Anal. calcd. for C₂₂H₂₁FN₄O (376.4354): C 70.20%, H 5.62%, N 14.88%. Found: C 69.84%, H 5.48%, N 14.83%.

4-((1*H*-Imidazol-1-yl)methyl)-1-(4-chlorophenyl)-3-(4-isopropoxyphenyl)-1*H*-pyrazole (11h). Prepared from 4-(chloromethyl)-1-(4-chlorophenyl)-3-(4-isopropoxyphenyl)-1*H*-pyrazole (**10h**) (0.30 g, 0.83 mmol). The pure compound was eluted with CH₂Cl₂-MeOH 97.5:2.5 v/v and obtained as a beige solid. Yield 0.30 g (94%), m.p. 98–100 °C, TLC (CH₂Cl₂-MeOH 95:5 v/v) R_f 0.45. ¹H NMR (DMSO-*d*₆): δ 8.52 (s, 1H, pyrazole), 7.90 (d, *J* = 9.0 Hz, 2H, Ar), 7.65 (s, 1H, imidazole), 7.58 (d, *J* = 9.0 Hz, 2H, Ar), 7.55 (d, *J* = 9.0 Hz, 2H, Ar), 7.13 (s, 1H, imidazole), 7.0 (d, *J* = 8.50 Hz, 2H, Ar), 6.89 (s, 1H, imidazole), 5.28 (s, 2H, CH₂-imidazole), 4.67 (m, 1H, CH), 1.30 (d, *J* = 6.0 Hz, 6H, 2 × CH₃). ¹³C NMR (DMSO-*d*₆): δ 158.06 (C, Ar), 150.96 (C, pyrazole), 138.61 (C, Ar), 137.48 (CH, imidazole), 130.82 (C, Ar), 130.01 (CH, imidazole), 129.95 (2 × CH, Ar), 129.29 (2 × CH, Ar), 129.10 (CH, pyrazole), 124.76 (C, pyrazole), 120.29 (2 × CH, Ar), 119.64 (CH, imidazole), 117.34 (C, Ar), 116.12 (2 × CH, Ar), 69.68 (CH), 40.98 (CH₂), 22.28 (2 × CH₃). Anal. calcd. for C₂₂H₂₁ClN₄O (392.1404): C 67.26%, H 5.39%, N 14.26%. Found: C 67.03%, H 5.16%, N 14.21%.

1-((1-(4-Fluorophenyl)-3-(4-methoxyphenyl)-1*H*-pyrazol-4-yl)methyl)-1*H*-1,2,4-triazole (12a). Prepared from 4-(chloromethyl)-1-(4-fluorophenyl)-3-(4-methoxyphenyl)-1*H*-pyrazole (**10a**) (0.44 g, 1.3 mmol). The pure compound was eluted with CH₂Cl₂-MeOH 97.5:2.5 v/v and obtained as an orange solid. Yield 0.26 g (58%), m.p. 150–152 °C, TLC (CH₂Cl₂-MeOH 95:5 v/v) R_f 0.63. ¹H NMR (DMSO-*d*₆): δ 8.54 (s, 1H, triazole), 8.54 (s, 1H, pyrazole), 7.99 (s, 1H, triazole), 7.90 (m, 2H, Ar), 7.67 (d, *J* = 8.50 Hz, 2H, Ar), 7.36 (m, 2H, Ar), 7.04 (d, *J* = 9.0 Hz, 2H, Ar), 5.48 (s, 2H, CH₂-triazole), 3.81 (s,

3H, CH₃). ¹⁹F NMR: (DMSO-*d*₆): -116.42 (F-Ar). ¹³C NMR (DMSO-*d*₆): δ 161.77 and 159.83 (d, ¹*J*_{CF} = 242.7 Hz, C-F, Ar), 159.80 (C, Ar), 151.99 (CH, triazole), 150.89 (C, pyrazole), 144.36 (CH, triazole), 136.39 and 136.36 (d, ⁴*J*_{CF} = 2.5 Hz, C, Ar), 130.40 (CH, pyrazole), 129.37 (2 × CH, Ar), 125.04 (C, pyrazole), 120.83 and 120.76 (d, ³*J*_{CF} = 8.7 Hz, 2 × CH, Ar), 116.86 and 116.68 (d, ²*J*_{CF} = 22.6 Hz, 2 × CH, Ar), 115.69 (C, Ar), 114.59 (2 × CH, Ar), 55.65 (CH₃), 43.81 (CH₂). Anal. calcd. for C₁₉H₁₆FN₅O (349.3694): C 64.99%, H 4.59%, N 19.94%. Found: C 64.67%, H 4.41%, N 19.95%.

1-((1-(4-Chlorophenyl)-3-(4-methoxyphenyl)-1*H*-pyrazol-4-yl)methyl)-1*H*-1,2,4-triazole (12b). Prepared from 4-(chloromethyl)-1-(4-chlorophenyl)-3-(4-methoxyphenyl)-1*H*-pyrazole (**10b**) (0.35 g, 1.05 mmol). The pure compound was eluted with CH₂Cl₂-MeOH 97:3 v/v and obtained as a light orange solid. Yield 0.32 g (60%), m.p. 124–126 °C, TLC (CH₂Cl₂-MeOH 95:5 v/v) R_f 0.65. ¹H NMR (DMSO-*d*₆): δ 8.59 (s, 1H, triazole), 8.54 (s, 1H, pyrazole), 7.99 (s, 1H, triazole), 7.90 (d, *J* = 9.0 Hz, 2H, Ar), 7.67 (d, *J* = 8.5 Hz, 2H, Ar), 7.58 (d, *J* = 9.0 Hz, 2H, Ar), 7.03 (d, *J* = 9.0 Hz, 2H, Ar), 5.48 (s, 2H, CH₂-triazole), 3.81 (s, 3H, CH₃). ¹³C NMR (DMSO-*d*₆): δ 159.87 (C, Ar), 152.01 (CH, triazole), 151.13 (C, pyrazole), 144.39 (CH, triazole), 138.58 (C, Ar), 130.90 (C, Ar), 130.37 (CH, pyrazole), 129.96 (2 × CH, Ar), 129.39 (2 × CH, Ar), 124.92 (C, pyrazole), 120.32 (2 × CH, Ar), 116.06 (C, Ar), 114.61 (2 × CH, Ar), 55.66 (CH₃), 43.79 (CH₂). Anal. calcd. for C₁₉H₁₆ClN₅O (365.8210): C 62.08%, H 4.39%, N 19.05%. Found: C 61.77%, H 4.14%, N 19.00%.

1-((3-(4-Ethoxyphenyl)-1-(4-fluorophenyl)-1*H*-pyrazol-4-yl)methyl)-1*H*-1,2,4-triazole (12c). Prepared from 4-(chloromethyl)-3-(4-ethoxyphenyl)-1-(4-fluorophenyl)-1*H*-pyrazole (**10c**) (0.40 g, 1.2 mmol). The pure compound was eluted with CH₂Cl₂-MeOH 98.5:1.5 v/v and obtained as a light brown solid. Yield 0.23 g (52%), m.p. 140–142 °C, TLC (CH₂Cl₂-MeOH 95:5 v/v) R_f 0.56. ¹H NMR (DMSO-*d*₆): δ 8.53 (s, 1H, pyrazole), 8.53 (s, 1H, triazole), 7.98 (s, 1H, triazole), 7.90 (m, 2H, Ar), 7.66 (d, *J* = 9.0 Hz, 2H, Ar), 7.36 (t, *J* = 8.50 Hz, 2H, Ar), 7.02 (d, *J* = 9.0 Hz, 2H, Ar), 5.48 (s, 2H, CH₂-triazole), 4.08 (q, *J* = 7.0 Hz, 2H, OCH₂), 1.35 (t, *J* = 7.0 Hz, 3H, CH₃). ¹⁹F NMR: (DMSO-*d*₆): -116.44 (F-Ar). ¹³C NMR (DMSO-*d*₆): δ 161.76 and 159.82 (d, ¹*J*_{CF} = 243.9 Hz, C-F, Ar), 159.08 (C, Ar), 151.99 (CH, triazole), 150.91 (C, pyrazole), 144.36 (CH, triazole), 136.39 and 136.37 (d, ⁴*J*_{CF} = 2.5 Hz, C, Ar), 130.37 (CH, pyrazole), 129.36 (2 × CH, Ar), 124.90 (C, pyrazole), 120.81 and 120.74 (d, ³*J*_{CF} = 8.80 Hz, 2 × CH, Ar), 116.85 and 116.67 (d, ²*J*_{CF} = 22.6 Hz, 2 × CH, Ar), 115.68 (C, Ar), 115.02 (2 × CH, Ar), 63.57 (OCH₂), 43.81 (triazole-CH₂), 15.11 (CH₃). Anal. calcd. for C₂₀H₁₈FN₅O (363.3964): C 66.10%, H 4.99%, N 19.26%. Found: C 66.21%, H 4.87%, N 19.17%.

1-((1-(4-Chlorophenyl)-3-(4-ethoxyphenyl)-1*H*-pyrazol-4-yl)methyl)-1*H*-1,2,4-triazole (12d). Prepared from 4-(chloromethyl)-1-(4-chlorophenyl)-3-(4-ethoxyphenyl)-1*H*-pyrazole (**10d**) (0.49 g, 1.41 mmol). The pure compound was eluted with CH₂Cl₂-MeOH 98:2 v/v and obtained as a light brown solid. Yield 0.32 g (60%), m.p. 122–124 °C, TLC (CH₂Cl₂-MeOH 95:5 v/v) R_f 0.49. ¹H NMR (DMSO-*d*₆): δ 8.58 (s, 1H, triazole), 8.54 (s, 1H, pyrazole), 7.98 (s, 1H, triazole), 7.90



(d, $J = 8.5$ Hz, 2H, Ar), 7.66 (d, $J = 9.0$ Hz, 2H, Ar), 7.57 (d, $J = 9.0$ Hz, 2H, Ar), 7.01 (d, $J = 9.0$ Hz, 2H, Ar), 5.48 (s, 2H, CH₂-triazole), 4.08 (q, $J = 7.0$ Hz, 2H, CH₂CH₃), 1.35 (t, $J = 6.5$ Hz, 3H, CH₂CH₃). ¹³C NMR (DMSO-*d*₆): δ 159.15 (C, Ar), 152.01 (CH, triazole), 151.15 (C, pyrazole), 144.39 (CH, triazole), 138.58 (C, Ar), 130.89 (C, Ar), 130.34 (CH, pyrazole), 129.96 (2 \times CH, Ar), 129.39 (2 \times CH, Ar), 124.78 (C, pyrazole), 120.31 (2 \times CH, Ar), 116.05 (C, Ar), 115.04 (2 \times CH, Ar), 63.58 (CH₂CH₃), 43.80 (CH₂), 15.11 (CH₂CH₃). Anal. calcd. for C₂₀H₁₈ClN₅O (379.8480): C 63.24%, H 4.78%, N 18.43%. Found: C 62.91%, H 4.63%, N 18.29%.

1-((1-(4-Fluorophenyl)-3-(4-propoxyphenyl)-1H-pyrazol-4-yl)methyl)-1H-1,2,4-triazole (12e). Prepared from 4-(chloromethyl)-1-(4-fluorophenyl)-3-(4-propoxyphenyl)-1H-pyrazole (**10e**) (0.30 g, 0.87 mmol). The pure compound was eluted with CH₂Cl₂-MeOH 98.5 : 1.5 v/v and obtained as a light orange solid. Yield 0.185 g (58%), m.p. 120–122 °C, TLC (CH₂Cl₂-MeOH 95 : 5 v/v) R_f 0.51. ¹H NMR (DMSO-*d*₆): δ 8.53 (s, 1H, pyrazole), 8.53 (s, 1H, triazole), 7.98 (s, 1H, triazole), 7.90 (m, 2H, Ar), 7.66 (d, $J = 9.0$ Hz, 2H, Ar), 7.36 (t, $J = 9.0$ Hz, 2H, Ar), 7.03 (d, $J = 9.0$ Hz, 2H, Ar), 5.48 (s, 2H, CH₂-triazole), 3.98 (t, $J = 6.5$ Hz, 2H, OCH₂), 1.76 (m, 2H, CH₂), 1.0 (t, $J = 7.0$ Hz, 3H, CH₃). ¹⁹F NMR (DMSO-*d*₆): δ -116.45 (F-Ar). ¹³C NMR (DMSO-*d*₆): δ 161.76 and 159.82 (d, $^1J_{CF} = 243.9$ Hz, C-F, Ar), 159.24 (C, Ar), 151.99 (CH, triazole), 150.91 (C, pyrazole), 144.36 (CH, triazole), 136.39 and 136.37 (d, $^4J_{CF} = 2.5$ Hz, C, Ar), 130.37 (CH, pyrazole), 129.36 (2 \times CH, Ar), 124.90 (C, pyrazole), 120.81 and 120.75 (d, $^3J_{CF} = 7.5$ Hz, 2 \times CH, Ar), 116.86 and 116.67 (d, $^2J_{CF} = 23.9$ Hz, 2 \times CH, Ar), 115.68 (C, Ar), 115.06 (2 \times CH, Ar), 69.46 (OCH₂), 43.82 (triazole-CH₂), 22.50 (CH₂), 10.88 (CH₃). Anal. calcd. for C₂₁H₂₀FN₅O (377.4234): C 66.83%, H 5.34%, N 18.55%. Found: C 66.67%, H 5.20%, N 18.67%.

1-((1-(4-Chlorophenyl)-3-(4-propoxyphenyl)-1H-pyrazol-4-yl)methyl)-1H-1,2,4-triazole (12f). Prepared from 4-(chloromethyl)-1-(4-chlorophenyl)-3-(4-propoxyphenyl)-1H-pyrazole (**10f**) (0.3 g, 0.83 mmol). The pure compound was eluted with CH₂Cl₂-MeOH 98.5 : 1.5 v/v and obtained as a light orange solid. Yield 0.23 g (72%), m.p. 114–116 °C, TLC (CH₂Cl₂-MeOH 95 : 5 v/v) R_f 0.69. ¹H NMR (DMSO-*d*₆): δ 8.58 (s, 1H, triazole), 8.54 (s, 1H, pyrazole), 7.98 (s, 1H, triazole), 7.91 (d, $J = 9.0$ Hz, 2H, Ar), 7.67 (d, $J = 9.0$ Hz, 2H, Ar), 7.58 (d, $J = 9.0$ Hz, 2H, Ar), 7.03 (d, $J = 9.0$ Hz, 2H, Ar), 5.48 (s, 2H, CH₂-triazole), 3.98 (t, $J = 6.5$ Hz, 2H, OCH₂), 1.76 (m, 2H, CH₂), 1.0 (t, $J = 7.0$ Hz, 3H, CH₃). ¹³C NMR (DMSO-*d*₆): δ 159.31 (C, Ar), 152.01 (CH, triazole), 151.15 (C, pyrazole), 144.40 (CH, triazole), 138.59 (C, Ar), 130.88 (C, Ar), 130.34 (CH, pyrazole), 129.96 (2 \times CH, Ar), 129.38 (2 \times CH, Ar), 124.78 (C, pyrazole), 120.31 (2 \times CH, Ar), 116.06 (C, Ar), 115.08 (2 \times CH, Ar), 69.47 (OCH₂), 43.81 (triazole-CH₂), 22.50 (CH₂), 10.88 (CH₃). Anal. calcd. for C₂₁H₂₀ClN₅O (393.8750): C 64.04%, H 5.12%, N 17.77%. Found: C 63.94%, H 5.02%, N 17.87%.

1-((1-(4-Fluorophenyl)-3-(4-isopropoxyphenyl)-1H-pyrazol-4-yl)methyl)-1H-1,2,4-triazole (12g). Prepared from 4-(chloromethyl)-1-(4-fluorophenyl)-3-(4-isopropoxyphenyl)-1H-pyrazole (**10g**) (0.15 g, 0.44 mmol). The pure compound was eluted with CH₂Cl₂-MeOH 98.5 : 1.5 v/v and obtained as

a light brown solid. Yield 0.088 g (53%), m.p. 118–120 °C, TLC (CH₂Cl₂-MeOH 95 : 5 v/v) R_f 0.52. ¹H NMR (DMSO-*d*₆): δ 8.54 (s, 1H, pyrazole), 8.53 (s, 1H, triazole), 7.99 (s, 1H, triazole), 7.90 (m, 2H, Ar), 7.65 (d, $J = 9.0$ Hz, 2H, Ar), 7.36 (t, $J = 9.0$ Hz, 2H, Ar), 7.01 (d, $J = 9.0$ Hz, 2H, Ar), 5.48 (s, 2H, CH₂-triazole), 4.67 (m, 1H, CH), 1.30 (d, $J = 6.0$ Hz, 6H, 2 \times CH₃). ¹⁹F NMR (DMSO-*d*₆): δ -116.46 (F-Ar). ¹³C NMR (DMSO-*d*₆): δ 161.75 and 159.82 (d, $^1J_{CF} = 242.7$ Hz, C-F, Ar), 158.03 (C, Ar), 152.0 (CH, triazole), 150.93 (C, pyrazole), 144.37 (CH, triazole), 136.39 and 136.37 (d, $^4J_{CF} = 3.77$ Hz, C, Ar), 130.33 (CH, pyrazole), 129.41 (2 \times CH, Ar), 124.74 (C, pyrazole), 120.80 and 120.73 (d, $^3J_{CF} = 8.8$ Hz, 2 \times CH, Ar), 116.86 and 116.67 (d, $^2J_{CF} = 23.9$ Hz, 2 \times CH, Ar), 116.10 (2 \times CH, Ar), 115.69 (C, Ar), 69.66 (CH), 43.82 (CH₂), 22.29 (CH₃). Anal. calcd. for C₂₁H₂₀FN₅O (377.4234): C 66.83%, H 5.34%, N 18.55%. Found: C 66.81%, H 5.16%, N 18.68%.

1-((1-(4-Chlorophenyl)-3-(4-isopropoxyphenyl)-1H-pyrazol-4-yl)methyl)-1H-1,2,4-triazole (12h). Prepared from 4-(chloromethyl)-1-(4-chlorophenyl)-3-(4-isopropoxyphenyl)-1H-pyrazole (**10h**) (0.3 g, 0.83 mmol). The pure compound was eluted with CH₂Cl₂-MeOH 97.5 : 2.5 v/v and obtained as a brown oil. Yield 0.26 g (81%), TLC (CH₂Cl₂-MeOH 95 : 5 v/v) R_f 0.48. ¹H NMR (DMSO-*d*₆): δ 8.57 (s, 1H, triazole), 8.54 (s, 1H, pyrazole), 7.99 (s, 1H, triazole), 7.91 (d, $J = 9.0$ Hz, 2H, Ar), 7.66 (d, $J = 9.0$ Hz, 2H, Ar), 7.58 (d, $J = 9.0$ Hz, 2H, Ar), 7.01 (d, $J = 9.0$ Hz, 2H, Ar), 5.48 (s, 2H, CH₂-triazole), 4.68 (m, 1H, CH), 1.30 (d, $J = 6.0$ Hz, 6H, 2 \times CH₃). ¹³C NMR (DMSO-*d*₆): δ 158.10 (C, Ar), 152.02 (CH, triazole), 151.16 (C, pyrazole), 144.40 (CH, triazole), 138.58 (C, Ar), 130.87 (C, Ar), 130.30 (CH, pyrazole), 129.96 (2 \times CH, Ar), 129.44 (2 \times CH, Ar), 124.61 (C, pyrazole), 120.29 (2 \times CH, Ar), 116.10 (2 \times CH, Ar), 116.06 (C, Ar), 69.67 (CH), 40.81 (CH₂), 22.29 (2 \times CH₃). HPLC: 97.0%, RT = 4.88 min. HRMS (ESI) *m/z*: calculated: 394.1435 [M + H]⁺, found: 394.1443 [M + H]⁺.

Mtb MIC assay

Spot culture growth inhibition (SPOTi) assay was performed as previously described.¹³ Briefly, each well of a flat 96-well plate was spotted with 2 μ L compound, serially diluted two-fold in DMSO from 150 μ g mL⁻¹. 200 μ L Middlebrook 7H10 agar supplemented with 0.5% (v/v) glycerol and 10% OADC was dispensed into each well of a flat 96-well plate and the plate shaken to homogenise the compound. The agar was allowed to set before storage at 4 °C and used in the SPOTi assay within 24 h. To inoculate the plate, *M. tuberculosis* H37Rv was first cultured with shaking at 37 °C in Middlebrook 7H9 media supplemented with 0.5% (v/v) glycerol, 10% OADC and 0.025% Tween 80 up to an OD of 1. The culture was then diluted 1 : 100 in 7H9 media and 2 μ L spotted onto each well of the SPOTi plate. Cultures were incubated at 37 °C for five weeks before MIC₉₀ was recorded for each compound.

CYP121A1 binding affinity assay

Recombinant CYP121A1 protein that was used in spectral binding assays was expressed and purified as described



previously.²⁴ Compounds were first screened for binding on a dual-beam Shimadzu 2700 spectrophotometer, in which ligand-free spectra of 1 μ M CYP121A1 (50 mM Tris HCl, 300 mM NaCl, pH 7.4) were compared with spectra in the presence of 250 μ M of each compound following a 15 min incubation period in a 1 cm quartz cuvette. The shape and intensity of preliminary difference spectra indicated peak maxima between 420–435 nm and minima between 380–415 nm and were consistent with a type-II ligand response.

Full titrations were performed in triplicate at ambient temperature using an Agilent BioTek Cytation 5 monochromator-based multimode plate reader. Protein samples at 1 μ M concentration and in 200 μ L volume were prepared in Corning® 96-well black flat bottom polystyrene 96 well plates. Individual wells were used to acquire 12 intermediate concentration points spanning 0 to 150 μ M of compound. K_d values were calculated by plotting the inhibitor concentrations against the blue-shifted type-II response. Data fitting was performed as described previously²⁴ using a single binding mode equation for hyperbolic fitting in Prism GraphPad v7.05. As additional controls, cYY substrate was included in the plate reader assay and all compounds were validated with a single manual titration on the Shimadzu 2700 spectrophotometer.

Protein expression, purification, and sample preparation for NMR

The mutant version of CYP121A1 protein containing C171S was expressed, purified, and labelled for NMR detection as described previously.¹⁸ Following purification, the protein was ¹⁹F labelled using 3-bromo-1,1,1-trifluoroacetone (BTFA). Briefly, the protein was diluted to 2 μ M in 50 mM Tris HCl, pH 7.4, and 300 mM NaCl supplemented with 10 mM BTFA and 5 mM DTT and incubated overnight at 4 °C. Unreacted BTFA and DTT were removed by size exclusion chromatography. The protein was exchanged into the NMR buffer (50 mM potassium phosphate, pH 7.4, 50 mM NaCl, and 10% D₂O) using a 10 kDa molecular weight cut-off filter. Protein was aliquoted into separate NMR samples at 100 μ M and 450 μ L volume. Compounds were added from a DMSO stock to a final concentration of 300 μ M and allowed to incubate for 15 min prior to transfer to NMR sample tubes. Spectra were acquired at 25 °C on a Bruker AVANCE III 600 MHz spectrometer for 10 000 scans per experiment. The data were processed and analyzed in TopSpin, version 4.1.1.

Computational studies

Molecular docking and molecular dynamics simulations were performed as previously described.^{25,26} Briefly docking studies, using the crystal structure of Mtb CYP121A1 co-crystallised with cYY (pdb 3G5H⁴) were performed to generate PDB Mtb CYP121A1–ligand complexes, using MOE²² until a RMSD gradient of 0.01 kcal mol^{−1} Å^{−1} with the MMFF94 forcefield (ligands) and partial charges were automatically calculated. The charge of the haem iron at physiological pH

was set to 3⁺ (geometry d²sp³) through the atom manager in MOE. Docking was performed using the Alpha Triangle placement to determine the poses, refinement of the results was done using the MMFF94 forcefield, and rescoring of the refined results using the London ΔG scoring function was applied. Molecular dynamics simulations were run on the Mtb CYP121A–ligand complexes as previously described²⁶ using the Desmond programme of Schöndinger.²³ Overlapping water molecules were deleted, and the systems were neutralised with Na⁺ ions and salt concentration 0.15 M. Force-field parameters for the complexes were assigned using the OPLS_2005 forcefield, that is, a 150 ns molecular dynamic run in the NPT ensemble (T 1/4 300 K) at a constant pressure of 1 bar. Energy and trajectory atomic coordinate data were recorded at each 1.2 ns.

Author contributions

Research concept designed by CS, DFE, SJW and SB. LAA performed the chemistry and analysis of all compounds supervised by CS. AK developed the methodology and performed the Mtb CYP121A1 and ¹⁹F NMR binding affinity studies supervised by DFE. SJW performed the SPOTi assay, with support and training from GS and SB. Computational studies and visualisation performed by CS. Manuscript reviewed by all authors.

Conflicts of interest

There are no conflicts to declare.

Acknowledgements

L. A. A. thanks Princess Nourah bint Abdulrahman University (College of Pharmacy, Department of Pharmaceutical Science) and the Royal Embassy of Saudi Arabia for a full PhD scholarship to complete this research at Cardiff University. Molecular dynamics simulations were undertaken using the supercomputing facilities at Cardiff University operated by Advanced Research Computing at Cardiff (ARCCA) on behalf of the Cardiff Supercomputing Facility and the HPC Wales and Supercomputing Wales (SCW) projects. We acknowledge support of the latter, which is part-funded by the European Regional Development Fund (ERDF) *via* the Welsh Government.

Notes and references

- 1 World Health Organisation, Global tuberculosis report 2021, <https://www.who.int/publications/i/item/9789240037021>, (accessed 23 March 2022).
- 2 J. L. Khawbung, D. Nath and S. Chakraborty, Drug resistant tuberculosis: a review, *Comp. Immunol., Microbiol. Infect. Dis.*, 2021, **74**, 101574.
- 3 K. J. McLean, A. J. Dunford, R. Neeli, M. D. Driscoll and A. W. Munro, *Arch. Biochem. Biophys.*, 2007, **464**, 228–240.



- 4 P. Belin, M. H. Le Du, A. Fielding, O. Lequin, M. Jacquet, J. B. Charbonnier, A. Lecoq, R. Thai, M. Courçon, C. Masson, C. Dugave, R. Genet, J. L. Pernodet and M. Gony, *Proc. Natl. Acad. Sci. U. S. A.*, 2009, **106**, 7426–7431.
- 5 K. J. Mclean, P. Carroll, D. G. Lewis, A. Dunford, H. E. Seward, R. Neeli, M. R. Cheesman, L. Marsollier, P. Douglas, W. E. Smith, I. Rosenkrands, S. T. Cole, D. Leys, T. Parish and A. W. Munro, *J. Biol. Chem.*, 2008, **283**, 33406–33416.
- 6 I. M. Taban, H. E. A. E. Elshihawy, B. Torun, B. Zucchini, C. J. Williamson, D. Altuwairigi, A. S. T. Ngu, K. J. McLean, C. W. Levy, S. Sood, L. B. Marino, A. W. Munro, L. P. S. de Carvalho and C. Simons, *J. Med. Chem.*, 2017, **60**, 10257–10267.
- 7 H. A. A. Abd El-wahab, M. Accietto, L. B. Marino, K. J. McLean, C. W. Levy, H. M. Abdel-Rahman, M. A. El-Gendy, A. W. Munro, A. S. Aboaraia and C. Simons, *Bioorg. Med. Chem.*, 2018, **26**, 161–176.
- 8 S. M. Kishk, K. J. McLean, S. Sood, M. A. Helal, M. S. Gomaa, I. Salama, S. Mostafa, L. P. S. de Carvalho, A. W. Munro and C. Simons, *Bioorg. Med. Chem.*, 2019, **27**, 1546–1561.
- 9 S. M. Kishk, K. J. McLean, S. Sood, D. Smith, J. W. D. Evans, M. A. Helal, M. S. Gomaa, I. Salama, S. Mostafa, C. W. Levy, L. P. S. de Carvalho, A. W. Munro and C. Simons, *ChemistryOpen*, 2019, **8**, 995–1011.
- 10 M. E. Kavanagh, J. L. Gray, S. H. Gilbert, A. G. Coyne, K. J. McLean, H. J. Davis, A. W. Munro and C. Abell, *ChemMedChem*, 2016, **11**, 1924–1935.
- 11 C. Brengel, A. Thomann, A. Schiffrin, G. Allegretta, A. A. M. Kamal, J. Haupenthal, I. Schnorr, S. H. Cho, S. G. Franzblau, M. Empting, J. Eberhard and R. W. Hartmann, *ChemMedChem*, 2017, **12**, 1616–1626.
- 12 I. Walter, S. Adam, M. V. Gentilini, A. M. Kany, C. Brengel, A. Thomann, T. Sparwasser, J. Köhnke and R. W. Hartmann, *ChemMedChem*, 2021, **16**, 2786–2801.
- 13 J. D. Guzman, D. Evangelopoulos, A. Gupta, K. Birchall, S. Mwaigwisya, B. Saxty, T. D. McHugh, S. Gibbons, J. Malkinson and S. Bhakta, *BMJ Open*, 2013, **3**, e002672.
- 14 J. A. Dijkstra, T. van der Laan, O. W. Akkerman, M. S. Bolhuis, W. C. M. de Lange, J. G. W. Kosterink, T. S. van der Werf, J. W. C. Alffenaar and D. van Soolingen, *Antimicrob. Agents Chemother.*, 2018, **62**, e01724.
- 15 A. K. Ghose and G. M. Crippen, *J. Chem. Inf. Comput. Sci.*, 1987, **27**, 21–35.
- 16 M. Fonvielle, M.-H. Le Du, O. Lequin, A. Lecoq, M. Jacquet, R. Thai, S. Dubois, G. Grach, M. Gondry and P. Belin, *J. Biol. Chem.*, 2013, **288**, 17347–17359.
- 17 H. E. Seward, A. Roujeinikova, K. J. McLean, A. W. Munro and D. Leys, *J. Biol. Chem.*, 2006, **281**, 39437–39443.
- 18 C. S. Campomizzi, G. E. Ghanatios and D. F. Estrada, *J. Biol. Chem.*, 2021, **297**, 101287.
- 19 P. Urban, T. Lautier, D. Pompon and G. Truan, *Int. J. Mol. Sci.*, 2018, **19**, 1617.
- 20 Y.-T. Lee, R. F. Wilson, I. Rupniewski and D. B. Goodin, *Biochemistry*, 2010, **49**, 3412–3419.
- 21 I. F. Sevrioukova and T. L. Poulos, *Proc. Natl. Acad. Sci. U. S. A.*, 2017, **114**, 486–491.
- 22 Molecular Operating Environment (MOE), Chemical Computing Group ULC, 2019, <https://www.chemcomp.com/Products.htm>.
- 23 Desmond Schrödinger Release 2020-1, Desmond Molecular Dynamics System, D.E. Shaw Research, New York, NY, Maestro Desmond Interoperability Tools, Schrödinger, New York, NY, 2020, <https://www.schrodinger.com/products/desmond>.
- 24 A. Kumar, C. S. Campomizzi, N. Jay, S. Ferguson, E.-J. Scheffler, J. Lioi, C. Tu, J. Qu, C. Simons and D. F. Estrada, *Sci. Rep.*, 2021, **11**, 394.
- 25 N. A. Noureldin, J. Richards, H. Kothayer, M. M. Baraka, S. M. Eladl, M. Wooton and C. Simons, *RSC Adv.*, 2022, **12**, 2511–2524.
- 26 F. A. Binjubair, J. E. Parker, A. G. Warrilow, K. Puri, P. J. Bradley, E. Tatar, S. L. Kelly, D. E. Kelly and C. Simons, *ChemMedChem*, 2020, **15**, 1294–1309.

